

Surface Recovery: Fusion of Image and Point Cloud

Siavash Hosseinyalamdary Alper Yilmaz
The Ohio State University
2070 Neil avenue, Columbus, Ohio, USA 43210
pcvlab.engineering.osu.edu

Abstract

The point cloud of the laser scanner is a rich source of information for high level tasks in computer vision such as traffic understanding. However, cost-effective laser scanners provide noisy and low resolution point cloud and they are prone to systematic errors. In this paper, we propose two surface recovery approaches based on geometry and brightness of the surface. The proposed approaches are tested in realistic outdoor scenarios and the results show that both approaches have superior performance over the state-of-art methods.

1. Introduction

Point cloud is a valuable source of information for scene understanding. There are scientific endeavors to detect and classify objects in a scene using Kinect point cloud [17]. In addition, urban challenge has proven that the point cloud, collected from laser scanner, is an essential source of information for reliable traffic understanding resulted in autonomous driving [19]. The accurate and high resolution laser scanners are expensive and may not be cost-effective to be used in autonomous vehicles. In contrast, point cloud generated from inexpensive laser scanners are noisy and low resolution and prone to systematic errors. Therefore, 3D scene recovery based on sparse and noisy point clouds has attracted scientific attentions. Independently, scientists has also attempted to reconstruct the surface of objects based on the images for many years. In this paper, we combine these two sources of information to recover the surface of the objects and remove the noise from the point cloud. Figure 1 shows the sparse point cloud collected by laser scanner overlaid on the image.

Surface of an object can be implicitly or explicitly represented in three dimensional Euclidean space. In explicit representation, a function is fitted to the sampled points of the surface. The Delaunay triangulation is the earliest attempt to explicitly represent the surface using triangles. Moreover, splines and its derivatives [18] are applied to re-

construct surfaces. Implicit (or volumetric) representation of a surface divides the three dimensional Euclidean space to voxels and the value of each voxel is defined based on an indicator function which describes the distance of the voxel to the surface. The value of every voxel inside the surface has negative sign, the value of the voxels outside the surface is positive and the surface is represented as zero crossing values of the indicator function. Unfortunately, this representation is not applicable to open surfaces and some modifications should be applied to reconstruct open surfaces. The least squares and partial differential equations (PDE) based approaches have also been developed to implicitly reconstruct surfaces. The moving least squares (MLS) [22, 1] and Poisson surface reconstruction [16], has been used in this paper for comparison, are particularly popular. Lim and Haron review different surface reconstruction techniques in more details [20]. Berger *et al.* also describe the advantages of different methods to handle noise, sparsity, missing data and misalignment in the point cloud and they investigate different applications of surface reconstruction [3].

Beside point cloud, the surface can be recovered from image content, known as shape from shading. The seminal works of Horn and his colleagues have initiated shape from shading approaches [13, 15]. This problem has been extensively studied for the laboratory environments where the different illuminations, light sources, object properties, and pose of the cameras are known [28, 7]. However, this problem has still remained unsolved for realistic scenarios where the surface reflectance and light source properties are unknown.

This paper relates the surface curvature and the brightness changes on the surface and introduces a cost function to minimize their difference. Consequently, a regularizer is constructed based on this cost function and it is used to recover the surface. Due to the complexity of the lighting situation, the regularizer cannot obtain satisfactory results unless it is updated by the sampled points of the surface.



Figure 1. This paper uses the image (left) and point cloud (right) sources to reconstruct the surface.

2. Methodology

A local coordinate system is defined at every sampled point to locally represent the surface of an object. We propose geometry and brightness based approaches to recover the surface at the neighborhood of the sampled points. The geometry based approach has been previously described in [14]. Finally, we introduce a global constraint to remove the discontinuities between locally estimated surfaces and assure continuity of the surface.

2.1. Local coordinate system

Every surface is a two dimensional manifold embedded into the three dimensional Euclidean space, $S : R^2 \rightarrow \Lambda \subset R^3$. Λ is a subset of R^3 that encompasses the surface. If we assume that the surface of the object is smooth and consequently differentiable, it becomes a Riemannian manifold and the tangent space, T , can be defined.

Let's assume that point \mathbf{X} is given on the surface and the normal vector of the surface, \vec{n} , is known at point \mathbf{X} . Let's define two orthonormal vectors \vec{u} and \vec{v} in the tangent space. Local coordinate system is defined in the way that its origin is located at point \mathbf{X} and its bases are the \vec{u} , \vec{v} , and \vec{n} . Let's define $\Omega_{\mathbf{X}}$ the neighborhood of the point \mathbf{X} on the surface and assume there is a point $\mathbf{X}' \in \Omega_{\mathbf{X}}$ on the surface at the neighborhood of point \mathbf{X} . The coordinates of point \mathbf{X}' is $\mathbf{X}' = [u_{\mathbf{X}'}, v_{\mathbf{X}'}, w_{\mathbf{X}'}]^T$. $w_{\mathbf{X}'}$ is the distance of the point \mathbf{X}' from the tangent space and it can be written as a function of the point coordinates in tangent space, u and v such that $W(u_{\mathbf{X}'}, v_{\mathbf{X}'}) = w_{\mathbf{X}'}$. W is a scalar field which indicated the distance of every point from the surface to the tangent space. In order to recover the surface, it suffices that the scalar field W is estimated in the neighborhood of point \mathbf{X} . The estimation of W is independent of the definition of two vector bases \vec{u} and \vec{v} . Here, we simplify the definition of W by choosing the following transformation between the local coordinate system, defined for the neighborhood of point \mathbf{X} , and Euclidean coordinate system, such that

$$\mathbf{X}' = \mathbf{R}_1(\alpha)\mathbf{R}_2(\beta)\mathbf{X}'_{\text{Euclidean}}. \quad (1)$$

If n_1, n_2 , and n_3 are elements of \vec{n} in 3D Euclidean space, it leads to $\alpha = -\arctan(\frac{n_2}{n_3})$ and $\beta = \arccos \sqrt{n_2^2 + n_3^2}$. \mathbf{R}_1 and \mathbf{R}_2 are rotations around \vec{X} and \vec{Y} axes of Euclidean coordinate system. This transformation transfers origin of

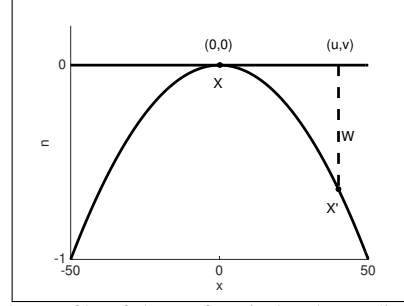


Figure 2. The profile of the surface in local coordinate system is presented in this figure. The sampled point \mathbf{X} on the surface is the origin of the local coordinate system and first and second axes of the local coordinate system are laid on the tangent space, \vec{u} and \vec{v} . Every point on the surface, \mathbf{X}' , has two components, u and v on the tangent space and one component in normal direction, W . Point \mathbf{X}' can be stated with $\mathbf{X}' = [u, v, W(u, v)]$ in the local coordinate system.

Euclidean coordinate system to the point \mathbf{X} and it maps \vec{X} , \vec{Y} , and \vec{Z} of Euclidean coordinate system into \vec{u} , \vec{v} , and \vec{n} of the local coordinate system. Figure 2 shows a profile of the surface where it is passed through point \mathbf{X} and point \mathbf{X}' . The tangent space is defined at point \mathbf{X} and point \mathbf{X}' can be recovered if $W(u_{\mathbf{X}'}, v_{\mathbf{X}'})$ is estimated.

In order to estimate $W(u_{\mathbf{X}'}, v_{\mathbf{X}'})$, point \mathbf{X} and its normal vector are not sufficient and other sampled point of the surface should be projected to the local coordinate system. Let's assume, the sampled points of the surface in the neighborhood of point \mathbf{X} are $\Pi = \{\mathbf{X}^1, \dots, \mathbf{X}^n\}$. The moving least squares (MLS) fits a polynomial to the sampled points in the local coordinate system to recover the surface. The disadvantage of MLS is that it assumes the neighborhood is the same in all directions. Therefore, it may violate the boundaries of the surface. We propose an approach to define the neighborhood based on geometry of the sampling points to preserve the boundaries.

Geometry of the surface at the local neighborhood can be represented as the co-variance matrix of the sampled points. The co-variance matrix, $\mathbf{S}_{\mathbf{X}\mathbf{X}} = \sum_{\mathbf{X}^i \in \Omega_{\mathbf{X}}} (\mathbf{X}^i - \mathbf{X})^T (\mathbf{X}^i - \mathbf{X})$ represents a three-dimensional ellipsoid. The axes of the ellipsoid are eigenvectors, $(\theta_1, \theta_2, \theta_3)$ of the matrix $\mathbf{S}_{\mathbf{X}\mathbf{X}}$ corresponding to the eigenvalues, $(\lambda_1 \geq \lambda_2 \geq \lambda_3 \geq 0)$, of this matrix. The normal to the surface at point \mathbf{X} is corresponding to the eigenvector θ_3 , with the smallest eigenvalues, λ_3 . Two other eigenvectors, θ_1, θ_2 , are corresponding to the two largest eigenvalues $\lambda_1 \geq \lambda_2$, indicate an ellipse in the tangent space. The ellipse follows geometry of the surface in the tangent space. That is, it become a circle within the boundaries of the surface and it elongates at the boundaries of the surface. Therefore, this definition of the neighborhood of

point \mathbf{X} does not violate the boundaries of the surface and consequently, it preserves the boundaries. Figure 3 shows our definition of the neighborhood of point \mathbf{X} in the tangent space.

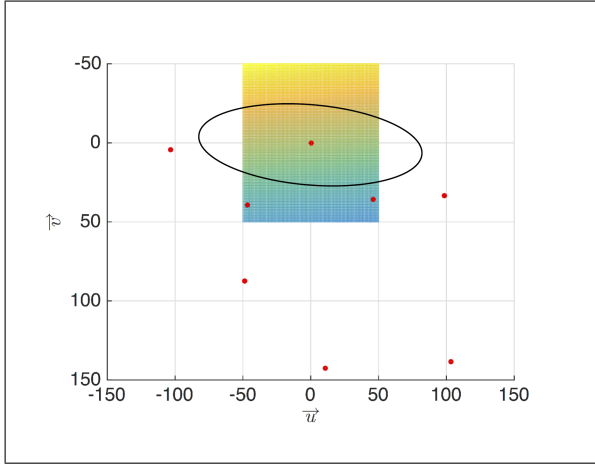


Figure 3. The neighborhood of point \mathbf{X} , corresponding to the highlighted region in Figure 1, is shown in the tangent space. A 100×100 grid is created around point \mathbf{X} and the other sampled points (red dots) are also projected to the tangent space. An ellipse is created based on the distribution of sampled points around point \mathbf{X} and the neighborhood of point \mathbf{X} is defined as the intersection of the grid points and ellipse. In other words, the grid points that lay in the ellipse belong to the neighborhood of point \mathbf{X} . The color of the grid points shows slope of the initial surface at this neighborhood.

2.2. Surface recovery based on geometry

In section 2.1, the local coordinate system is defined at point \mathbf{X} . If the scalar field W is estimated in the neighborhood of point \mathbf{X} , the surface can be recovered in this neighborhood. However, estimation of the scalar field W is an inverse problem and it cannot be estimated without any assumption. For instance, it is assumed that the surface is planar in the Voronoi triangulation and a plane is fitted into every three points of the surface. Here, we assume that the surface is smooth and therefore, $\nabla W \simeq 0$, where $\nabla = [\frac{\partial}{\partial u}, \frac{\partial}{\partial v}]$. This assumption leads to the cost function and the smoothness of the surface is guaranteed by minimizing the energy of this cost function, such that

$$\min_{W: \Omega \rightarrow R} E(W) = \iint_{\Omega} \phi(\|\nabla W\|) dudv, \quad (2)$$

$\Phi(\cdot)$ is an arbitrary differentiable convex function and $\|\nabla W\|$ is L_2 norm of ∇W . The Euler-Lagrange equations can be applied to minimize (2) and it leads to isotropic diffusion equation if $\Phi(\cdot)$ is a quadratic function, such that

$$\frac{\partial W}{\partial t} = \text{div}(\nabla W) \quad (3)$$

Solution of this equation is a uniform gaussian filter that provides a smooth surface. The disadvantage of this method is that it smoothes the corners and edges of the surface since it is uniform gaussian filter. In order to preserve the corners and edges, the diffusion tensor, D , can be introduced into (3), such that

$$\frac{\partial W}{\partial t} = \text{div}(D\nabla W) \quad (4)$$

Equation (4) is anisotropic diffusion equation which its solution is equivalent to the oriented gaussian filter. In order to preserve the edges and corners, D should be selected in the way that it suppresses the smoothing filter in the direction of ∇W . The choice of diffusion tensor has been extensively studied in image processing [27, 25, 23]. The solution of (2) can be estimated using the gradient descent in an iterative scheme

$$W_{k+1} = W_k - \frac{\partial W}{\partial t} \delta, \quad (5)$$

where the subscripts indicate to the iterations and δ is the step size in the gradient descent iterative solution. Obviously, an initial estimate of the surface, W_0 , is required in (5) to estimate the surface in the next iterations.

In (4), the sampled points do not change if $\frac{\partial W}{\partial t} = 0$ for the sampled points. Depending on the accuracy of the sampled points, an additional term is added in (4) to handle noise in the sampling points, such that

$$\begin{cases} \frac{\partial W}{\partial t} = \text{div}(D\nabla W) & \text{if } \mathbf{X}' \notin \mathbf{X}^i \\ \frac{\partial W}{\partial t} = \epsilon & \text{if } \mathbf{X}' \in \mathbf{X}^i. \end{cases} \quad (6)$$

$\epsilon \leq 0$ is a parameter dependent on the accuracy of the sampling points. If $\epsilon = 0$, then (6) obtains a smooth surface in the way that it passes through the sampling points. If the sampled points of the surface are noisy, then by the choice of $\epsilon > 0$ the sampling points are smoothed by the rate of ϵ .

2.3. Surface recovery based on reflectance

The idea of using reflectance of an object to recover the surface is not new and shape from shading has been studied to reconstruct the surface of an object for many years. The reflectance is a function of light source energy, its direction, the surface normal vector and its material. This function is called Bidirectional Reflectance Distribution Function (BRDF). Like geometry, reflectance based surface reconstruction is an inverse problem and therefore, it is ill-conditioned. In the controlled environment where the lighting sources are known, such as photometric stereo, different illuminations are used to reconstruct the surface. Furthermore, the shade cue has been used with other cues, such as motion cue, to resolve this ill-condition problem. In an inspiring work, the motion cue estimated from optical flow is integrated with the shade cue to reconstruct the surface [5, 4].

If image of an object is available, the brightness of the image depends on the reflectance of the object. In order to recover the surface based on reflectance, the lighting sources, the material of surface and its optics properties, and the camera pose should be known. In a realistic uncontrolled indoor and outdoor scenarios, when these sources of information are not available, it is impossible to recover the surface. Here, we assume convexity of the surface, distant illumination and orthographic light source. The distant illumination and orthographic light source assumption is especially valid for outdoor environment. If the surface is recovered in a local coordinate system, the convexity assumption of the surface is valid for the neighborhood of point \mathbf{X} .

Let's assume the tangent space is tangential to the surface at point \mathbf{X} , point \mathbf{X}' is a point on the surface in $\Omega_{\mathbf{X}}$, and the brightness of these points is $I(\mathbf{x})$ and $I(\mathbf{x}')$ in the image space. The brightness changes indicate the changes in normal direction of the surface at these points [26], such as

$$|I(\mathbf{x}) - I(\mathbf{x}')| \simeq \arccos(\vec{n}_{\mathbf{x}}^{\top} \vec{n}_{\mathbf{x}'}), \quad (7)$$

where $\vec{n}_{\mathbf{x}}$ and $\vec{n}_{\mathbf{x}'}$ are normal vectors to the surface at points \mathbf{X} and \mathbf{X}' . The normal vectors at point \mathbf{X} and point \mathbf{X}' in the local coordinate system are $\vec{n}_{\mathbf{x}} = [0, 0, 1]^{\top}$ and $\vec{n}_{\mathbf{x}'} = \frac{1}{\mu} [W_u, W_v, 1]^{\top}$ where $\mu = \sqrt{1 + W_u^2 + W_v^2}$. Replacing normals in (7), it can easily be shown that

$$\|\nabla W\| \simeq \tan |I(\mathbf{x}) - I(\mathbf{x}')|. \quad (8)$$

Equation (8) constructs a cost function that relates the surface changes in the local coordinate system to the brightness changes in the image. By minimizing the energy of cost function (8), the surface can be recovered, such that

$$\min_{W: \Omega \rightarrow \mathbb{R}} E(W) = \iint_{\Omega} \Phi(\|\nabla W\| - \tan |I(\mathbf{X}) - I(\mathbf{X}')|) dudv. \quad (9)$$

The Euler-Lagrange equations provide the necessary conditions for the minimization of (9), such that

$$\frac{\partial W}{\partial t} = \text{div}(\Phi(\|\nabla W\| - \tan |I(\mathbf{x}) - I(\mathbf{x}')|) \frac{\nabla W}{\|\nabla W\|}). \quad (10)$$

If the brightness changes are small, $\tan |I(\mathbf{x}) - I(\mathbf{x}')| \simeq 0$ and (10) is converted to the uniform gaussian filter in (3). When the brightness changes are significant (10) becomes anisotropic diffusion equation and the rate of the diffusion in each direction is equivalent to the brightness changes in that direction. In other words, brightness changes indicates to the curvature on the surface. Similar to geometry based surface recovery, the sampled points can be smoothed if these points are noisy, such that

$$\begin{cases} \frac{\partial W}{\partial t} = \text{div}(\Phi(\|\nabla W\| - \tan |I(\mathbf{x}) - I(\mathbf{x}')|) \frac{\nabla W}{\|\nabla W\|}) & \text{if } \mathbf{X}' \notin \mathbf{X}^i \\ \frac{\partial W}{\partial t} = \epsilon & \text{if } \mathbf{X}' \in \mathbf{X}^i. \end{cases} \quad (11)$$

It should be noted that the noise in the image can cause incorrect surface changes and therefore, the recovered surface may not be smoothed using the noisy images. Therefore, it is suggested that noise is removed from the image by applying filters, such as bilateral filter. Also, it is assumed that the brightness changes are the results of the surface curvature. However, the brightness can change due to the texture and it may affect the results of the surface recovery. It may required that the surface recovery is suppressed in the presence of texture.

2.4. Global constraint

When the surface in the neighborhood of point \mathbf{X} is recovered, it can be transferred to Euclidean coordinate system using (1). The surface of an object is recovered when the local surfaces of all neighborhoods of sampled points are transferred to Euclidean coordinate system. However, it does not guarantee a continuous surface of an object since the local surfaces are independently estimated. Therefore, a global constraint is required to provide a continuous surface from the independently estimated local surfaces. A Markov random field regularizer can be used to impose the global smoothness constraint, such that

$$\min_{\Lambda} E(S) = \sum_{X^i} (S(X^i) - X^i)^2 + \int_{\Lambda} S(X)^2 dX, \quad (12)$$

where Λ is the subset of R^3 that encompasses the surface. The surface, $S(X)$ in (12) is a function that represents the surface of the object. In order to satisfy the global continuity constraint, we have designed a filter to remove discontinuities of the surface in the normal direction such that,

$$\begin{cases} w = \int \exp\left(\frac{(X' - X)\vec{n}}{\|X' - X\|}\right) dX' \\ X_{\vec{n}} = \int w X'_{\vec{n}} dX'. \end{cases} \quad (13)$$

where \vec{n} is the normal direction of the surface at point \mathbf{X} . Equation (13) indicates that points of the surface are smoothed in the normal direction. This equation smoothes the corners and edges too.

2.5. Numerical scheme

Equation (2) provides a smooth surface of the object. However, the solution to this equation is not feasible in reality and the problem cannot be solved unless the surface is discretized and this equation is estimated for finite points of the surface. Therefore, we consider that surface at the local neighborhood is a 100×100 grid and the location of these grid points are estimated based on geometry or brightness in previous sections.

The given solution may obtain incorrect results in the lack of numerical conditioning. Let's assume the local coordinate system is defined for the point \mathbf{X} with the neighborhood $\Omega_{\mathbf{X}}$. Based on [12, 11], the distance between points

should be scaled in the way that the maximum distance of the grid points in this neighborhood changes to $\sqrt{2}$. If the point \mathbf{X} is not located in the center of the grid points, the centroid of the grid points in the neighborhood should be estimated and the origin of coordinate system should be shifted to the centroid.

In addition, (6) and (11) minimize the cost function in an iterative way and therefore, the initial is required to be updated in every step. In order to approximate the surface of the object, we fit a second order polynomial to the sampled points in the neighborhood. In some regions that sufficient sampled points do not exist, we have applied lower orders of polynomials.

3. Experiment

In order to evaluate the proposed approaches, we have used a point cloud collected by laser scanner in one epoch. Therefore, the point cloud represents the part of object which is visible from the laser scanner perspective and it is an open surface. Some of objects in the scene may have holes. For instance, laser passes through windows on the van in the dataset and the observed point cloud has few holes. Topology of a surface indicates the number of holes in the surface. In geometry based surface recovery, we have only used the laser scanner point cloud, but in reflectance based surface recovery, the image taken by a camera on the platform and the laser scanner point cloud are integrated to reconstruct the surface. The images are taken from PointGray Flea2 color camera and the point clouds are collected from Velodyne HDL-64E laser scanner in KITTI dataset [9, 8]. The sampled points are 2 centimeters accurate in range, they are sampled in 0.09° angular resolution and they are within 120 meters range [9, 8]. The images are 1.4 Megapixels, 90° opening angle and global shutter. The camera and laser scanner are calibrated and external and internal calibration parameters of the sensors are known.

The evaluation of the surface recovery is still an open problem for realistic datasets. Ideally, two surfaces have the identical points. However, it is not valid for the real surfaces and there may not exist the corresponding points between two surfaces. Berger *et al.* (2003) pointed out to this problem when they compare the recovered surfaces to the benchmark. Arguably, if the distance between the recovered surface and the benchmark surface are small, the surface recovery is assumed to be successful. Berger *et al.* have provided a benchmark and compared existing surface recovery approaches [2] and concluded that Moving Least Squares (MLS) and its variants, such as Algebraic Point set surfaces (APSS) [10] and Robust Implicit Moving Least Squares (RIMLS) [21], have superior performance over the other approaches [2]. Unfortunately, the image of objects is not given in [2] and the proposed approaches cannot be evaluated by this benchmark. Therefore, we compare our

algorithm with Poisson, MLS, APSS, RIMLS surface reconstruction approaches in a realistic outdoor scenario. It is attempted to use the same set of parameters for these surface recovery approaches and the proposed approach in this paper.

4. Results

In the proposed approaches in section 2.2 and 2.3, surface is recovered in the neighborhood of the sampled points in the local coordinate system. Figure 4 demonstrates the proposed approaches at the neighborhood of one of these sampled points. The neighborhood is highlighted by red rectangle in Figure 1. Figure 4a shows the cropped image corresponding to this neighborhood. Figure 4b demonstrates an initial planar estimation of the surface and it can be seen that the surface does not correctly fit to the sampled points in this neighborhood. In Figure 4c, geometry based surface recovery (4) is used to reconstruct the surface. Equation (4) guarantees that the surface passes through the sampled points. If the sampled points are noisy, surface can be recovered in the way that the sampled points are smoothed too. Equation (6) is applied to suppress noise in the sampled points in Figure 4d. Figure 4e illustrates surface recovery based on the brightness (10). In this case, the brightness discontinuity leads to surface discontinuity. Like geometry based surface recovery, the sampled points can be smoothed in brightness based surface recovery. Equation (11) is used to suppress noise of the sampled points and generate the surface in Figure 4f.

In the local coordinate system, the local surface is estimated for every local neighborhood and the locally estimated surfaces are transferred to global (Euclidean) coordinate system. Therefore, the local surfaces may not fit to each other and the generated surface may become discontinuous. Therefore, the global constraint is applied to guarantee the final surface is smooth. Figure 5a demonstrate the results of the surface recovery using brightness and Equation (13) is used to guarantee the surface smoothness in Figure 5b. Figure 5a and 5b may look similar, but the zoomed look in bottom row demonstrates that the global constraint provides a smooth surface. However, the global constraint is computationally expensive and may not be used in near realtime applications.

In Figure 4, the proposed approaches are evaluated for a local surface. We compare the proposed approaches for the whole surface in Figure 6. The first row shows the surface from sensor's perspective and the second row shows top view of the surface. Figure 6 shows that initial surface, geometry based surface recovery, and brightness based surface recovery can reconstruct the surface. It can be seen that the proposed approaches do not fill in the holes (such as windows of the van) of the surface and they preserve the topology.

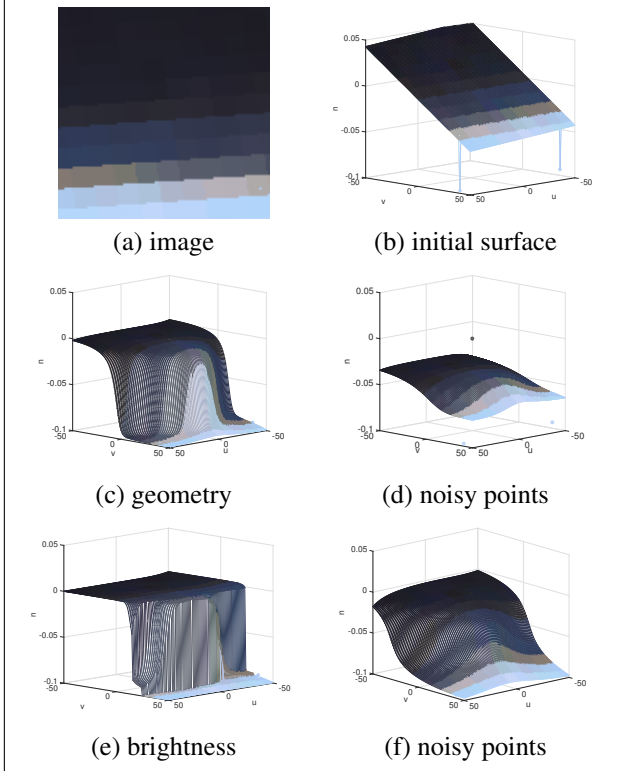


Figure 4. (a) The cropped image corresponding to the neighborhood of point X. This neighborhood is highlighted with a red rectangle in Figure 1; (b) The surface is approximated by fitting a plane in this neighborhood. This surface is used as initial surface for (4), (6), (10) and (11). (c) The local surface is recovered based on pure geometry according to (4). Equation (4) enforces that the estimated surface must pass through the sampled points. (d) If the sampled points are noisy, the estimated surface may not pass through these points. The estimated surface can filter the sampled points according to (6). (e) The brightness regularizer in (10) obtains a smooth surface that passes through the sampled points. (f) If the sampled points are noisy, (11) can be used to provide a smooth surface.

According to [2] moving least squares approach and its variants have superior performance over the other surface recovery approaches. Poisson and MLS surface recovery approaches has been implemented using point cloud library (PCL) [24] in this paper. In Poisson approach, a mesh based surface of the object is created and the points are sampled from the generated mesh based surface. The surface is generated from fitting the second order polynomial to the local surfaces in MLS. The search radius and up-sampling radius are 50 centimeters. Two variants of MLS, APSS and RIMLS, have been implemented using MeshLab [6]. Filter scale is 2 for both methods, the spherical parameter is 1 in APSS and the maximum fitting iterations is 3 in RIMLS. It is attempted to provide the same resolution for all of the approaches. However, these algorithms have different strategies and the resolution may not be the same. Figure 7 shows

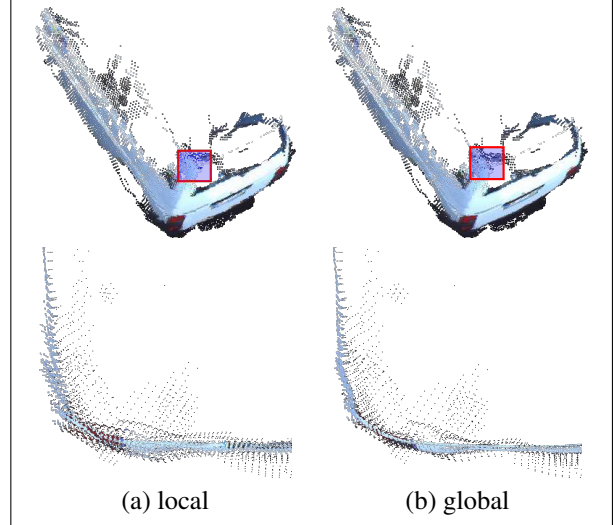


Figure 5. The highlighted part of the first row is zoomed in the second row. (a) The locally estimated surfaces are transferred to the global coordinate system and the estimated surface may become discontinuous. (b) If the global smoothness is applied, the surface becomes continuous.

the results of the surface recovery for these four approaches. These approaches fill in the holes (windows of the car) of the object and cannot preserve the topology. The boundary of the surface is also violated and the shape of the object is distorted.

In Figure 4, initial surface, geometry based surface recovery, and brightness based surface recovery show similar performance in large scale view. Figure 8 shows the results of the propose surface recovery approaches for a complex object. The object, cyclist, is close to the sensor, it has a complex surface, it is adversely affected by motion of the platform during data collection. Figure 8 shows that brightness based surface recovery has superior performance over initial surface and geometry based surface recovery and it obtains a smoother and more realistic surface.

5. Conclusions

In this paper, we propose geometry based and brightness based surface recovery. The proposed algorithms are tested for a realistic scenario when the camera and laser scanner are mounted on a moving vehicle. The results show that both of geometry based and brightness based surface recovery approaches outperform the state of art surface reconstruction approaches. In addition, a global constraint is provided to smooth the discontinuities of the locally estimated surfaces and guarantee the continuity of the surface. In contrast to the existing approaches, the proposed approaches preserve the boundary of objects and keep the topology of surfaces.

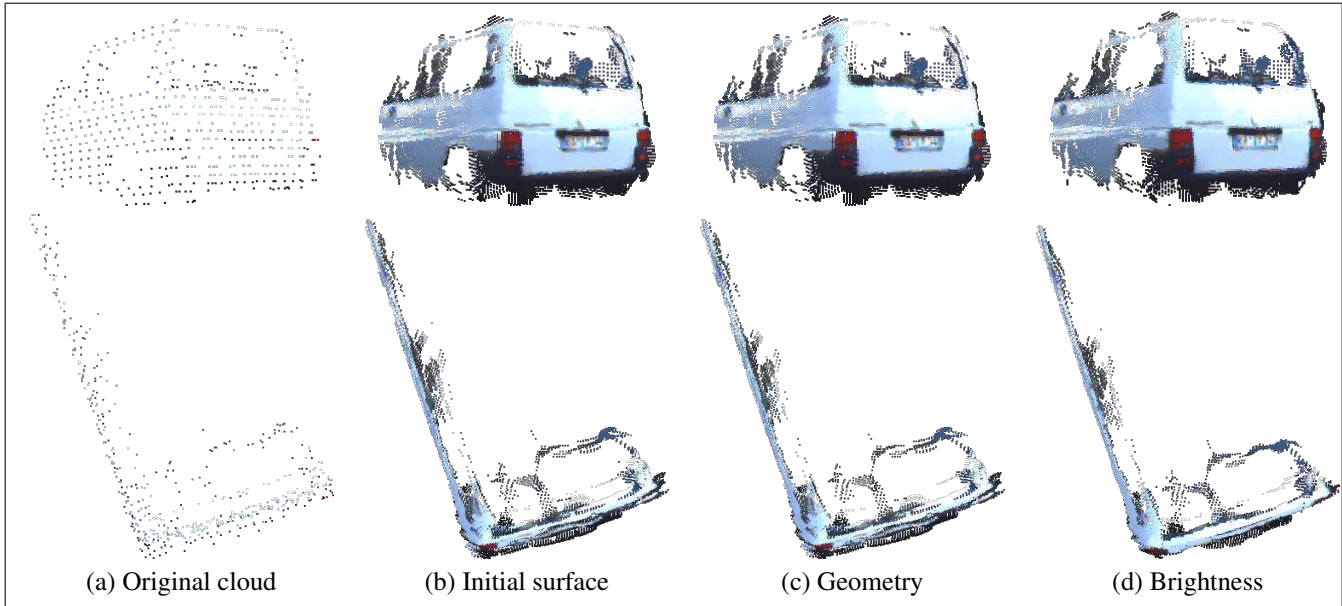


Figure 6. The proposed surface recovery approaches in sensor’s perspective (top row) and top view (bottom row); (a) The original point cloud, (b) Initial surface based on fitting the second order polynomial, (c) Geometry based surface recovery, (d) Brightness based surface recovery. It is shown that the initial surface, geometry based surface reconstruction, and brightness based surface recovery can provide a smooth and realistic surface. In the large scale, these three methods provide similar results for this object.

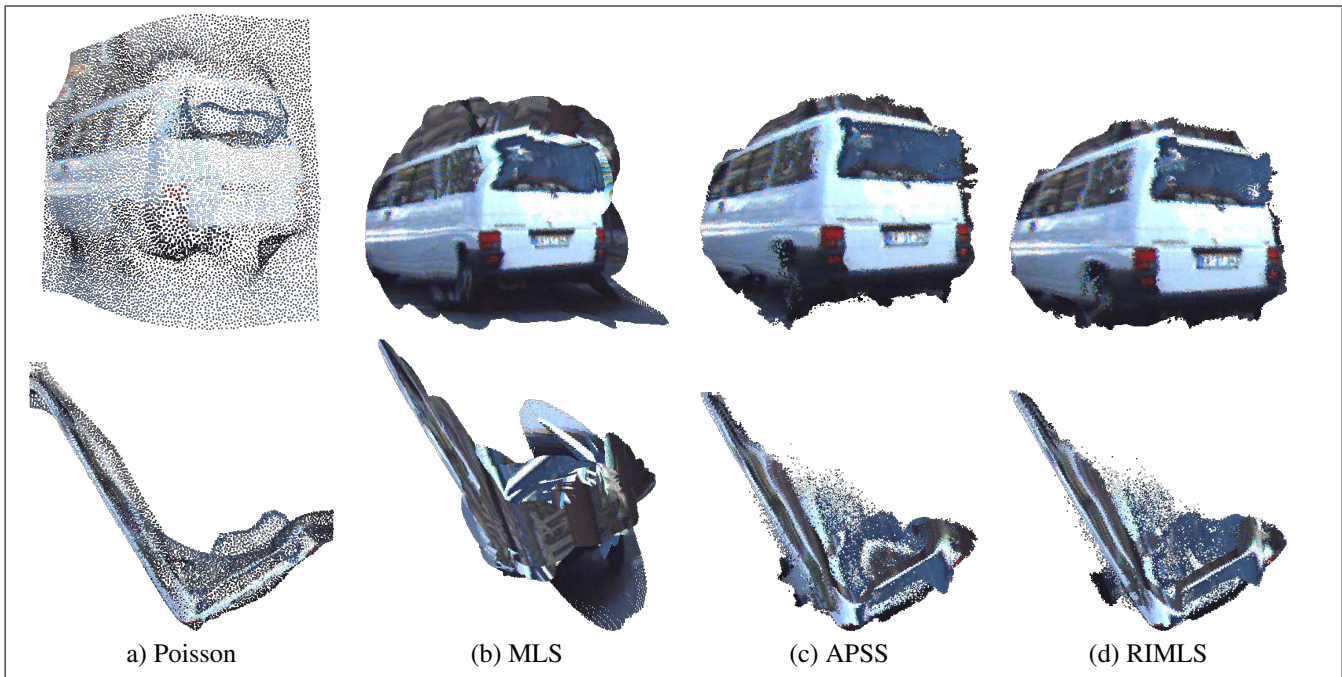


Figure 7. A few existing surface recovery approaches in sensor’s perspective (top row) and top view (bottom row); (a) Poisson based surface recovery [16], (b) Moving least squares surface recovery [22, 1], (c) Algebraic point set surfaces approach [10], (d) Robust implicit moving least squares method [21]. Top view of the generated surfaces shows that none of these method can provide a smooth and realistic surface. The boundary of the object is violated and the shape of the object is distorted in all these methods.

References

- [1] M. Alexa, J. Behr, D. Cohen-Or, S. Fleishman, D. Levin, and C. T. Silva. Computing and rendering point set surfaces.

IEEE Transactions on Visualization and Computer Graphics, 9(1):3–15, 2003.

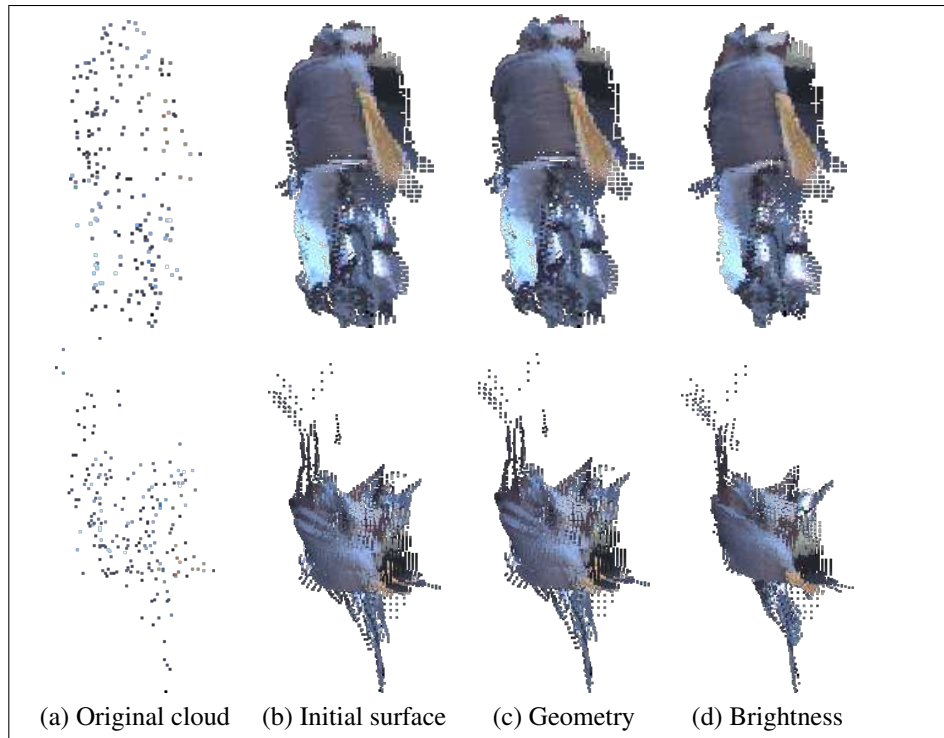


Figure 8. The proposed surface recovery approaches in sensor’s perspective (top row) and top view (bottom row) evaluated for a complex surface; (a) Original point cloud, (b) Initial surface based on fitting second order polynomial, (c) Geometry based surface recovery, (d) Brightness based surface recovery. Brightness based surface reconstruction has superior performance over geometry based surface recovery.

[2] M. Berger, J. A. Levine, L. G. Nonato, G. Taubin, and C. T. Silva. A benchmark for surface reconstruction. *ACM Transactions on Graphics*, 32(2):20:1–20:17, 2013.

[3] M. Berger, A. Tagliasacchi, L. M. Seversky, P. Alliez, J. A. Levine, A. Sharf, and C. Silva. State of the art in surface reconstruction from point clouds. *Eurographics STAR*, 2014.

[4] M. Chandrakar. On shape and material recovery from motion. In *European Conference on Computer Vision*, 2014.

[5] M. Chandrakar. What camera motion reveals about shape with unknown brdf. In *Conference on Computer Vision and Pattern Recognition*, 2014.

[6] P. Cignoni, M. Corsini, and G. Ranzuglia. Meshlab: an open-source 3d mesh processing system. *The European Research Consortium for Informatics and Mathematics (ERCIM) News*, 2008(73), 2008.

[7] J. Durou, M. Falcone, and M. Sagona. Numerical methods for shape-from-shading: A new survey with benchmarks. *Computer Vision and Image Understanding*, 109(1):22–43, 2008.

[8] A. Geiger, P. Lenz, C. Stiller, and R. Urtasun. Vision meets robotics: The kitti dataset. *International Journal of Robotics Research*, 2013.

[9] A. Geiger, P. Lenz, and R. Urtasun. Are we ready for autonomous driving? the kitti vision benchmark suite. In *Conference on Computer Vision and Pattern Recognition*, 2012.

[10] G. Guennebaud and M. Gross. Algebraic point set surfaces. *ACM Transactions on Graphics*, 26(3), 2007.

[11] R. I. Hartley. In defense of the eight-point algorithm. *IEEE Transactions on Pattern Analysis and Machine Intelligence*, 19(6):580–593, 1997.

[12] R. I. Hartley and A. Zisserman. *Multiple View Geometry in Computer Vision*. Cambridge University Press, ISBN: 0521540518, second edition, 2004.

[13] B. K. P. Horn. *The Psychology of Computer Vision*, chapter Obtaining shape from shading information, pages 115–155. McGraw-Hill, New york, 1975.

[14] S. Hosseinyalamdary and A. Yilmaz. 3d super-resolution approach for sparse laser scanner data. In *ISPRS Annals of the Photogrammetry, Remote Sensing and Spatial Information Sciences*, volume II-3/W5, pages 151–157, 2015.

[15] K. Ikeuchi and B. K. P. Horn. Numerical shape from shading and occluding boundaries, 1981.

[16] M. Kazhdan, M. Bolitho, and H. Hoppe. Poisson surface reconstruction. In *Proceedings of the fourth Eurographics symposium on Geometry processing*, pages 61–70, 2006.

[17] K. Lai, L. Bo, and D. Fox. Unsupervised feature learning for 3d scene labeling. In *IEEE International Conference on on Robotics and Automation*, 2014.

[18] S. Lee, G. Wolberg, and S. Y. Shin. Scattered data interpolation with multilevel b-splines scattered data interpolation with multilevel b-splines scattered data interpolation with multilevel b-spline. *IEEE Transactions on Visualization and Computer Graphics*, 3(3):228–244, 1997.

- [19] J. Levinson, J. Askeland, J. Becker, J. Dolson, D. Held, S. Kammel, J. Z. Kolter, D. Langer, O. Pink, V. Pratt, M. Sokolsky, G. Stanek, D. Stavens, A. Teichman, M. Werling, and S. Thrun. Towards fully autonomous driving: systems and algorithms. In *Intelligent Vehicles Symposium (IV)*, 2011.
- [20] S. P. Lim and H. Haron. Surface reconstruction techniques: a review. *Artificial Intelligence Review*, 42(1):59–78, 2014.
- [21] A. C. Öztireli, G. Guennebaud, and M. Gross. Feature preserving point set surfaces based on non-linear kernel regression. *Computer Graphics Forum*, 28(2):493–501, 2009.
- [22] M. Pauly, R. Keiser, L. P. Kobbelt, and M. Gross. Shape modeling with point-sampled geometry. In *ACM SIG-GRAPH*, pages 641–650, 2003.
- [23] P. Perona and J. Malik. Scale-space and edge detection using anisotropic diffusion. *IEEE Transactions on Pattern Analysis and Machine Intelligence*, 12(7):629–639, 1990.
- [24] R. B. Rusu and S. Cousins. 3D is here: Point Cloud Library (PCL). In *IEEE International Conference on Robotics and Automation*, 2011.
- [25] G. Sapiro. *Geometric Partial Differential Equations and Image Analysis*. Cambridge University Press, New York, NY, USA, 2006.
- [26] I. Sato, T. Okabe, Q. Yu, and Y. Sato. Shape reconstruction based on similarity in radiance changes under varying illumination. In *International Conference on Computer Vision*, pages 1–8, 2007.
- [27] D. Tschumperlé and R. Deriche. Vector-valued image regularization with pdes: A common framework for different applications. *IEEE Transaction on Pattern Analysis and Machine Intelligence*, 27(4):506–517, 2005.
- [28] R. Zhang, P. Tsai, J. E. Cryer, and M. Shah. Shape from shading: A survey. *IEEE Transactions on Pattern Analysis and Machine Intelligence*, 21(8):690–706, 1999.